JOURNAL OF GUIDANCE, CONTROL, AND DYNAMICS
Vol. 31, No. 6, November–December 2008

Artificial Three-Body Equilibria for Hybrid Low-Thrust Propulsion

Shahid Baig* and Colin R. McInnes†
University of Strathclyde, Glasgow G1 1XJ, Scotland, United Kingdom

DOI: 10.2514/1.36125

This paper proposes a new concept of creating artificial equilibrium points in the circular restricted three-body problem, in which the third body uses a hybrid of solar sail and solar electric propulsion. The work aims to investigate the use of a hybrid sail for artificial equilibrium points that are technologically difficult with either of these propulsion systems alone. The hybrid sail has the freedom of specifying the sail lightness number, then minimizing the required thrust acceleration from the solar electric propulsion thruster while satisfying the equilibrium condition. The stability analysis of such artificial equilibrium points by a linear method results in a linear time-varying (mass) system. The freezing-time method then provides unstable and marginally stable regions for hybrid solar sail artificial equilibria. We compare these propulsion systems with a given payload mass and mission life for a polar observation mission. For a near-term sail assembly loading, we find for the hybrid sail a substantially lower propellant mass compared with solar electric propulsion, a lower sail length with respect to a solar sail, and a lower initial spacecraft mass.

Nomenclature

A_S = sail area (not including thin-film area)
A_T = total hybrid sail area, $A_S + A_{\mathrm{TF}}$
A_{TF} = thin-film area
$\mathbf{a}_{\mathrm{gc}}$ = nondimensional required acceleration vector to balance gravitational and centrifugal forces
a_{gc} = magnitude of vector $\mathbf{a}_{\mathrm{gc}}$
$\acute{a}_{\mathrm{gc}}$ = dimensional required acceleration to balance gravitational and centrifugal forces, $a_{\mathrm{ref}} \times a_{\mathrm{gc}}$
a_{ref} = dimensional reference acceleration, 0.00593 $\mathrm{m/s^2}$ in the sun–Earth system
a_s = nondimensional acceleration magnitude due to solar radiation pressure for a hybrid sail
a_T = nondimensional thrust acceleration from the electric propulsion system of the hybrid sail
$\acute{a}_T$ = dimensional thrust acceleration from the electric propulsion system of the hybrid sail,$a_{\mathrm{ref}} \times a_T$
$\mathbf{C}_{b/a}$ = transformation matrix from the a to b frame
c = speed of flight, 3×10^8 m/s
G = universal gravitational constant, 6.672×10^{-11} $\mathrm{N\,m^2/kg^2}$
g_0 = gravity constant at the Earth's surface, 9.81 $\mathrm{m/s^2}$
L_s = solar luminosity
m = instantaneous mass of the hybrid sail
m_1 = mass of the sun
m_2 = mass of the Earth
p_i = ith polynomial coefficient of the cubic equation, $(i = 0 - 2)$
R_1 = dimensional distance between the sun and the hybrid sail
$\mathbf{r}$ = position vector of the hybrid sail with respect to the center of mass of the two primaries
$\tilde{r}_S$ = sail film reflectivity
$\tilde{r}_{\mathrm{TF}}$ = thin-film reflectivity
r_1 = nondimensional distance between the sun and the hybrid sail
T = thrust from the solar electric propulsion system of the hybrid sail, N
Δt = time step
$\sigma*$ = critical sail loading parameter, 1.53×10^{-3} $\mathrm{kg/m^2}$
τ_m = mission lifetime
ω = dimensional angular velocity of the rotating frame, $\sqrt{\frac{G(m_1+m_2)}{R^3}}$ $\mathrm{s^{-1}}$
$\boldsymbol{\omega}$ = nondimensional angular velocity vector of the rotating frame

Received 10 December 2007; revision received 6 March 2008; accepted for publication 2 April 2008.

*Ph.D. Candidate, Department of Mechanical Engineering; shahid.baig@strath.ac.uk.
†Professor, Department of Mechanical Engineering; colin.mcinnes@strath.ac.uk. Member AIAA.

I. Introduction

FIVE natural equilibrium points exist in the classical circular restricted three-body problem (CRTBP). These points are the Lagrange points where gravitational and centrifugal forces acting on a spacecraft in a rotating frame are balanced. Artificial equilibrium points (AEPs) similar to Lagrange points can be generated if continuous constant acceleration is available from a low-thrust propulsion system such as solar sail or solar electric propulsion (SEP). The continuous acceleration from either of these propulsion systems cancels any residual acceleration at the AEP, so that a static equilibrium point can be generated or a periodic orbit around the AEP if the eigenvalue spectrum of the AEP contains at least one center. For a solar sail, incident and reflected solar photons transfer momentum to a large and lightweight reflective membrane and so by adding a low-thrust continuous acceleration in the CRTBP, McInnes et al. [1] showed that continuous surfaces of unstable AEPs are generated. These AEPs are characterized by a sail lightness number (or total sail loading) and sail orientation. McInnes [2] in subsequent studies finds, for a realistic, partially reflecting sail for which the acceleration vector is no longer strictly normal to the sail surface, a reduction in the volume of artificial equilibrium solutions attached to the natural L_1 and L_2 Lagrange points. Morrow et al. [3] carried out an analysis for a solar sail hovering in close proximity to an asteroid and found the AEP solutions in Hill's problem similar to the restricted three-body problem. Baoyin and McInnes [4] reconsidered the AEP solutions for a solar sail in the elliptical restricted three-body problem and found that equilibrium points exist only within the ecliptic plane. However, the authors find that when the eccentricity of the orbit of the primary bodies is small, out of ecliptic equilibria can be achieved with active control. Other studies [5,6] have suggested periodic orbits around these AEPs in and above the ecliptic plane for the solar sail CRTBP. The NASA/National Oceanic and Atmospheric Administration (NOAA) Geostorm Warning mission

is an application of solar sail equilibria in the ecliptic plane and is based on a sail assembly loading of 14 g/m^2 (a key sail technology parameter) and a sail size of 100 × 100 m [7]. NOAA interest [8] in polar observer missions [9,10] uses an application of sail equilibria out of the ecliptic plane. However, for a polar observer mission, a sail with the same sail assembly loading as for the Geostorm mission needs a large sail (>175 × 175 m). The deployment and control of such a large solar sail will be technologically difficult. Improvements in two key sail design parameters, a decrease in the sail assembly loading and an increase in sail length, are being developed [11].

For an SEP system, in which the reaction mass provides a low-thrust propulsive force, Morimoto et al. [12] found artificial equilibrium points (unstable and marginally stable) in the CRTBP. These AEPs are characterized by the low-thrust acceleration magnitude and thrust orientation. Morimoto et al. [13] also found resonant periodic orbits at the linear order around the marginally stable points along the axis joining the primary bodies with a constant, continuous acceleration. However, continuous acceleration from an SEP system at AEPs for several years will require a large mass of propellant fraction, unlike a sail that is a true propellantless system.

In this paper, we investigate a new concept for creating AEPs in the CRTBP using these two low-thrust propulsion systems (solar sail and SEP) simultaneously. Such a hybrid of sail/SEP spacecraft is termed a hybrid sail. We find that a hybrid sail can be in equilibrium in forbidden regions for a pure sail. In particular, we consider a polar observer mission and compare the hybrid sail, pure SEP, and pure sail systems with a given payload mass and mission life time. We find that, in the case of a hybrid sail with the same sail assembly loading as for the Geostorm mission, a substantially lower sail length with respect to a pure sail system and a lower propellant mass and maximum electric power with respect to a pure SEP system is required.

The idea of the hybrid sail was apparently first proposed by Leipold and Götz [14], who assumed a square sail and an SEP thruster attached to the sail center, with part of the sail area at the sail center covered by flexible thin-film solar cells (TFSC). TFSC will act as a power source for the SEP system and other subsystems of the hybrid sail. TFSC technology has many advantages over state-of-the-art wafer-based solar cell technology including a high power/mass ratio, low cost, and good resistance against radiation. To qualify TFSC for future space use, flight experiments are being planned in low Earth orbit and medium Earth orbit [15]. Leipold and Götz [14] and recently Mengali and Quarta [16] in their studies showed that the hybrid sail has an attractive feature of reducing mission time with respect to a pure sail and a pure SEP system, respectively, for heliocentric transfers.

In the next section we describe the total force model for a partially reflecting hybrid sail. The solar radiation pressure (SRP) and SEP accelerations are normalized with respect to a reference acceleration and are used in Sec. III to describe the equations of motion of a hybrid sail in the CRTBP. For a hybrid sail, we find freedom in specifying the sail lightness number at a given AEP and minimizing the required SEP acceleration while satisfying the equilibrium condition. Two strategies are discussed to maintain the equilibrium condition. In Sec. IV, because of the slowly time-varying (mass) linear system, the freezing-time method is used to determine the stability of AEPs of a hybrid sail in the sun–Earth CRTBP. Section V compares the performance of the hybrid sail relative to a pure sail and a pure SEP system for a polar Earth observer mission. Finally, conclusions are presented in Sec. VI.

II. Partially Reflecting Hybrid Sail Model

A. Dimensional Force Model

The hybrid sail configuration is adopted from Leipold and Götz [14] as described in the previous section. They developed a hybrid sail force model that takes different reflectivities for the sail and TFSC area for their magnitude, but leaves the thrust direction acting normal to the sail surface. This paper considers a hybrid sail model that has an SRP force component along the sail surface (nonideal reflectivity), and so the total SRP force is no longer normal to the sail surface.

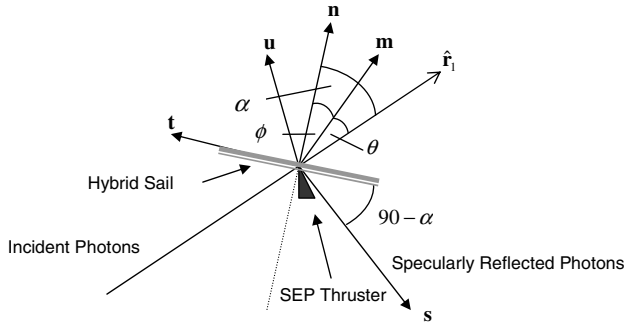

Fig. 1 Solar radiation pressure force model for a specularly reflecting hybrid sail. The solar electric propulsion thruster is also shown.

The solar radiation pressure at a distance R_1 from the sun is given by

$$P = L_s/4\pi R_1^2 c \tag{1}$$

The unit vectors normal and transverse to the hybrid sail surface are defined by $\mathbf{n}$ and $\mathbf{t}$, respectively, as shown in Fig. 1. The direction of incident photons is described by $\hat{\mathbf{r}}_1 = \cos\alpha\mathbf{n} - \sin\alpha\mathbf{t}$, and so the SRP force due to the incident photons is then

$$\mathbf{F}_i = PA_T \cos\alpha(\hat{\mathbf{r}}_1) \tag{2}$$

where $A_T \cos\alpha$ is the projected area in the direction of the incident photons. We assume specular reflection (no diffuse reflection and thermal reemission) from both the TFSC area A_{TF} and sail area A_S. The force on the hybrid sail due to the reflected photons is then

$$\mathbf{F}_r = \tilde{r}_S PA_S \cos\alpha(-\mathbf{s}) + \tilde{r}_{\mathrm{TF}} PA_{\mathrm{TF}} \cos\alpha(-\mathbf{s}) \tag{3}$$

The unit vector $\mathbf{s} = -\cos\alpha\mathbf{n} - \sin\alpha\mathbf{t}$ defines the direction of the specularly reflected photons. The total force exerted on the hybrid sail due to incident and reflected photons is therefore

$$\mathbf{F}_S = F_n\mathbf{n} + F_t\mathbf{t} \tag{4}$$

with

$$F_n = (\hat{\mathbf{r}}_1.\mathbf{n})^2[(1+\tilde{r}_S)PA_S + (1+\tilde{r}_{\mathrm{TF}})PA_{\mathrm{TF}}]$$

$$F_t = (\hat{\mathbf{r}}_1.\mathbf{n})(\hat{\mathbf{r}}_1.\mathbf{t})[(1-\tilde{r}_S)PA_S + (1-\tilde{r}_{\mathrm{TF}})PA_{\mathrm{TF}}]$$

where $\hat{\mathbf{r}}_1.\mathbf{n} = \cos\alpha$ and $\hat{\mathbf{r}}_1.\mathbf{t} = -\sin\alpha$, and so the SRP force on the hybrid sail $\mathbf{F}_S$ will now act in direction $\mathbf{m}$ as shown in Fig. 1.

The force due to the SEP thruster placed at the center of the sail, as shown in Fig. 1, is given by

$$\mathbf{F}_{\mathrm{SEP}} = T\mathbf{u} \tag{5}$$

where the unit vector $\mathbf{u}$ denotes the thrust direction.

The total thrust provided by the hybrid sail due to the SRP and the SEP thruster can be obtained from the sum of Eqs. (4) and (5).

B. Nondimensional Acceleration Model

In the CRTBP, a spacecraft of negligible mass m moves under the gravitational influence of the two primaries. The two primaries m_1 and m_2 orbit *circularly* with constant angular velocity ω in the (ecliptic) plane about their common center of mass. The unit of length is chosen such that the distance between the primaries R is taken to be unity and the unit of mass is chosen such that $G(m_1 + m_2) = 1$. If we define $\mu = m_2/(m_1 + m_2)$ as a nondimensional mass ratio, then in this system the gravitational constants are $Gm_2 = \mu$ and $Gm_1 = 1 - \mu$. The orbit period of the primary bodies is set to $\tau = 2\pi$. Thus, the nondimensional unit acceleration corresponds to $a_{\mathrm{ref}} = \omega^2 R = 0.00593$ m/s^2 in the sun–Earth system.

To obtain the acceleration $\mathbf{a}_S$ due to SRP for a hybrid sail in nondimensional form, which will be used in the equations of motion of the hybrid sail described in the next section, we divide Eq. (4) by mass m and the dimensional reference acceleration $\omega^2 R$. Then, rearranging, we have

$$\mathbf{a}_S = a_s\mathbf{m} = \frac{1}{2}\beta_0\frac{m_0}{m}\frac{1-\mu}{r_1^2}g(\hat{\mathbf{r}}_1.\mathbf{n})^2\mathbf{n} + \frac{1}{2}\beta_0\frac{m_0}{m}\frac{1-\mu}{r_1^2}h(\hat{\mathbf{r}}_1.\mathbf{n})(\hat{\mathbf{r}}_1.\mathbf{t})\mathbf{t} \tag{6}$$

where

$$g = (1+\tilde{r}_S) - (A_{\mathrm{TF}}/A_T)(\tilde{r}_S - \tilde{r}_{\mathrm{TF}})$$
$$h = (1-\tilde{r}_S) + (A_{\mathrm{TF}}/A_T)(\tilde{r}_S - \tilde{r}_{\mathrm{TF}})$$

and m_0 is the initial mass of the hybrid sail and $\beta_0 \equiv \sigma^*/(\frac{m_0}{A_T})$ is defined as the dimensionless lightness number. The acceleration model for a nonideal pure sail [2] is easily recovered from Eq. (6) when the sail mass is constant $m = m_0$ and $\tilde{r}_{\mathrm{TF}} = \tilde{r}_S$.

For a given m_0, β_0, and TFSC fractional area with respect to the total area, the *magnitude* of acceleration due to the SRP acting on the hybrid sail increases with the decrease of the hybrid sail mass m and may be written as

$$a_s = \frac{1}{2}\beta_0\frac{m_0}{m}\frac{1-\mu}{r_1^2}\sqrt{g^2\cos^2\alpha + h^2\sin^2\alpha}\cos\alpha \tag{7}$$

The offset angle between $\mathbf{m}$ and $\mathbf{n}$, usually called the centerline angle ϕ (see Fig. 1), can be obtained from Eq. (6) by dividing the ratio of the transverse and normal accelerations:

$$\tan\phi = (h/g)\tan\alpha \tag{8}$$

The actual *direction* of the SRP acceleration for a hybrid sail is defined by the cone angle θ. Using the relation $\alpha = \theta + \phi$ and Eq. (8), the cone angle θ can be written as

$$\tan\theta = \frac{(g-h)\tan\alpha}{g + h\tan^2\alpha} \tag{9}$$

We assume a reflectivity for a typical aluminized sail film $\tilde{r}_S = 0.9$ and for the TFSC area $\tilde{r}_{\mathrm{TF}} = 0.4$ [14]. Figure 2 shows that the maximum cone angle, $\theta_{\max} = 61$ deg, of the hybrid sail is less than the maximum cone angle, 64.15 deg, of a pure sail. This is due to the fact that for a hybrid sail $\tilde{r}_{\mathrm{TF}} < \tilde{r}_S$.

The nondimensional acceleration due to the SEP thruster can be obtained from Eq. (5) by dividing the hybrid sail mass m and reference acceleration a_{ref}:

$$\mathbf{a}_{\mathrm{SEP}} = \frac{T/m}{a_{\mathrm{ref}}}\mathbf{u} = a_T\mathbf{u} \tag{10}$$

These force models will now be used to define the sets of the AEP.

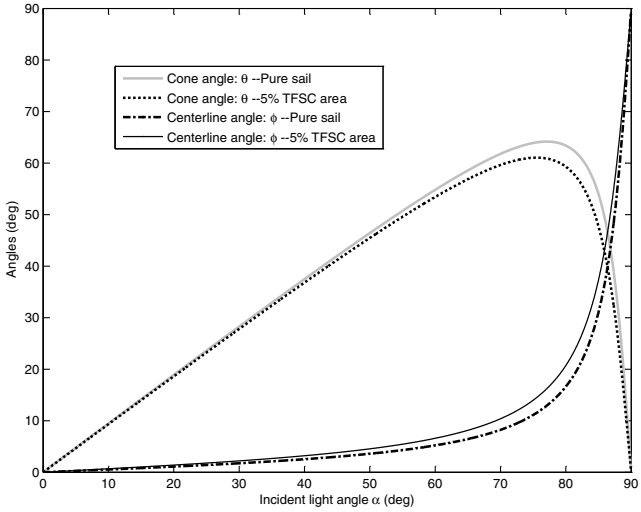

Fig. 2 Maximum cone angle for a hybrid sail (5% TFSC area with regard to total area) is less than that for a pure sail (with no TFSC area).

III. Equations of Motion and Artificial Equilibria

Consider a frame $F_a(x, y, z)$ corotating with the two primary masses at constant angular velocity $\boldsymbol{\omega}$ with the origin at their center of mass, as shown in Fig. 3. The x axis points along the sun–Earth line, the z axis is the axis of rotation, and the y axis completes the right-hand coordinate system. The nondimensional equation of motion of a hybrid sail in the rotating frame of reference F_a is given by

$$\frac{\mathrm{d}^2\mathbf{r}}{\mathrm{d}t^2} + 2\boldsymbol{\omega}\times\frac{\mathrm{d}\mathbf{r}}{\mathrm{d}t} + \boldsymbol{\omega}\times(\boldsymbol{\omega}\times\mathbf{r}) = -\nabla V + \mathbf{a}_S + \mathbf{a}_{\mathrm{SEP}} \tag{11}$$

where $\boldsymbol{\omega} = [0 \quad 0 \quad 1]^T$. The vectors $\mathbf{a}_S$ and $\mathbf{a}_{\mathrm{SEP}}$ are the accelerations due to solar radiation pressure and the solar electric propulsion system and may be written in the frame F_a as

$$\mathbf{a}_S = a_s\mathbf{m}^a, \qquad \mathbf{a}_{\mathrm{SEP}} = a_T\mathbf{u}^a \tag{12}$$

The three-body gravitational potential V is defined as

$$V = -\left[\frac{1-\mu}{r_1} + \frac{\mu}{r_2}\right] \tag{13}$$

where $\mathbf{r}_1 = [x+\mu \quad y \quad z]^T$ and $\mathbf{r}_2 = [x-(1-\mu) \quad y \quad z]^T$ are the position vectors of the hybrid sail with respect to the primary bodies. The centrifugal term in Eq. (11) can be written as

$$\nabla\Phi(\mathbf{r}) = \boldsymbol{\omega}\times(\boldsymbol{\omega}\times\mathbf{r}), \qquad \Phi(\mathbf{r}) = -\tfrac{1}{2}(x^2+y^2) \tag{14}$$

By defining a new scalar function $U(\mathbf{r}) = V(\mathbf{r}) + \Phi(\mathbf{r})$, the reduced equation of motion for the hybrid sail is obtained:

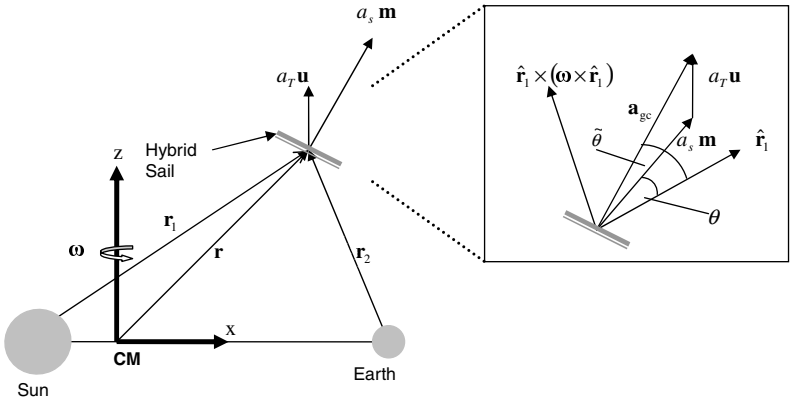

Fig. 3 Definition of the coordinate system and hybrid sail using two low-thrust propulsion systems.

$$\frac{\mathrm{d}^2\mathbf{r}}{\mathrm{d}t^2} + 2\boldsymbol{\omega} \times \frac{\mathrm{d}\mathbf{r}}{\mathrm{d}t} + \nabla U(\mathbf{r}) = \mathbf{a}_S + \mathbf{a}_{\mathrm{SEP}} \tag{15}$$

An artificial equilibrium point $\mathbf{r}_0$ in the rotating frame of reference F_a is obtained if the vector sum of the continuous low-thrust acceleration from the two propulsion systems satisfy the following equation:

$$\nabla U(\mathbf{r}_0) = \mathbf{a}_S + \mathbf{a}_{\mathrm{SEP}} \triangleq \mathbf{a}_{\mathrm{gc}} \tag{16}$$

Now $\nabla U(\mathbf{r}_0) = \mathbf{a}_{\mathrm{gc}}$ is the acceleration vector required to cancel the gravitational forces of the two primary bodies and the centrifugal force in the rotating frame F_a. It may also be defined as the acceleration required for converting a nonequilibrium point into an AEP at $\mathbf{r}_0$. For a pure sail system [1], the required acceleration vector is generated by the SRP acceleration vector alone whereas, for a pure SEP system [12], it is generated by the acceleration vector from the SEP system alone. For a hybrid sail, Eq. (16) shows that the required vector to keep the hybrid sail at AEP $\mathbf{r}_0$ is generated by the vector sum of the SRP and the SEP acceleration vectors. We now define a new frame F_b that will be useful in the next section to minimize the thrust acceleration from the SEP system. F_b is defined with a set of three orthogonal vectors $\{\mathbf{r}_1, \boldsymbol{\omega} \times \mathbf{r}_1, \mathbf{r}_1 \times (\boldsymbol{\omega} \times \mathbf{r}_1)\}$ and with its origin at the hybrid sail position. The rotation matrix from a to b can then be written as

$$\mathbf{C}_{b/a}(\mathbf{r}_0) = \left[\frac{\mathbf{r}_1}{|\mathbf{r}_1|} \quad \frac{\boldsymbol{\omega}\times\mathbf{r}_1}{|\boldsymbol{\omega}\times\mathbf{r}_1|} \quad \frac{\mathbf{r}_1\times(\boldsymbol{\omega}\times\mathbf{r}_1)}{|\mathbf{r}_1\times(\boldsymbol{\omega}\times\mathbf{r}_1)|} \right]^T \tag{17}$$

Therefore, the condition for artificial equilibrium Eq. (16) in F_b is given by

$$\mathbf{a}^{\,b}_{\mathrm{gc}} = a_s \mathbf{m}^b + a_T \mathbf{u}^b \tag{18}$$

where $\mathbf{a}^b_{\mathrm{gc}} = [\,a_1 \quad a_2 \quad a_3\,]^T = \mathbf{C}_{b/a} \nabla U(\mathbf{r_0})$. Equation (18) can now be rewritten as

$$a_T^2 = a_{\mathrm{gc}}^2 - 2a_s \mathbf{m}^b \cdot \mathbf{a}^b_{\mathrm{gc}} + a_s^2 \tag{19}$$

The required vector $\mathbf{a}_{\mathrm{gc}}$ to keep the hybrid sail at an AEP and the direction $\mathbf{m}$ that defines the direction of the SRP acceleration vector can be expressed in F_b according to Fig. 4 as

$$\mathbf{a}^{\,b}_{\mathrm{gc}} = a_{\mathrm{gc}} \begin{bmatrix} & \cos\tilde{\theta} \\ \sin\tilde{\theta} & \sin\tilde{\delta} \\ \sin\tilde{\theta} & \cos\tilde{\delta} \end{bmatrix}, \qquad \mathbf{m}^b = \begin{bmatrix} & \cos\theta \\ \sin\theta & \sin\delta \\ \sin\theta & \cos\delta \end{bmatrix} \tag{20}$$

where the cone angle $\tilde{\theta}$ and clock angle $\tilde{\delta}$ of $\mathbf{a}_{\mathrm{gc}}$ depend upon the AEP $\mathbf{r}_0$ and can be calculated as

$$\tilde{\theta} = \cos^{-1}(a_1/a_{\mathrm{gc}}) \tag{21}$$

$$\tilde{\delta} = \tan^{-1}(a_2, a_3) \tag{22}$$

Using Eq. (20) in Eq. (19), the low-thrust acceleration from the SEP system of the hybrid sail can be expressed in terms of the sail pitch angle α and the sail clock angle δ that defines the hybrid sail normal $\mathbf{n}$ as shown in Fig. 4:

$$a_T^2(\alpha, \delta) = a_{\mathrm{gc}}^2 - 2a_{\mathrm{gc}}a_s(\cos\theta\cos\tilde{\theta} + \sin\theta\sin\tilde{\theta}\cos(\delta - \tilde{\delta})) + a_s^2 \tag{23}$$

where a_s and θ are functions of the pitch angle α as given by Eqs. (7) and (9), respectively.

For a pure sail or a pure SEP system, the required acceleration magnitude and thrust orientation are completely defined by the location of the artificial equilibria $\mathbf{r}_0$. For a hybrid sail, the desired acceleration vector to keep the hybrid sail at an AEP is achieved by the sum of the SRP acceleration vector and the SEP acceleration vector, as shown in Fig. 3. By fixing β_0, $m = m_0$, Fig. 5 shows that there is freedom in selecting the orientation of the SRP acceleration direction to obtain the desired acceleration vector $\mathbf{a}_{\mathrm{gc}}$ while minimizing the SEP thrust. Once the optimum orientation is selected to obtain the maximum benefit from the SRP, the required orientation for the SEP thruster system $\mathbf{u}$ may be determined from the condition for artificial equilibria Eq. (18).

A. Minimization of SEP Acceleration at $t = 0$

The problem may now be formulated to determine the optimal hybrid sail cone and clock angles $(\alpha^*(0), \delta^*(0))$ to minimize the thrust acceleration a_T from the SEP system at an AEP $\mathbf{r}_0$ and for a given sail lightness number β_0. At initial time $t = 0$, $m = m_0$ and Eq. (7) becomes

$$a_s = a_s(0) = \frac{1}{2}\beta_0 \frac{1-\mu}{r_1^2} \sqrt{g^2\cos^2\alpha + h^2\sin^2\alpha}\cos\alpha \tag{24}$$

Using Eq. (24) in Eq. (23) and setting the derivative of a_T with respect to δ to zero yields a stationary point for the optimal clock angle:

$$\frac{\partial a_T}{\partial \delta} = a_{\mathrm{gc}} \frac{a_s(0)}{a_T} \sin\theta \sin\tilde{\theta} \sin(\delta - \tilde{\delta}) = 0 \tag{25}$$

With $\alpha \neq 90$ deg or $a_s(0) \neq 0$, $\theta \neq 0$, and $\tilde{\theta} \neq 0$, Eq. (25) holds if

$$\delta^*(0) = \tilde{\delta} \tag{26}$$

This states that the hybrid sail clock angle should be aligned with the clock angle of the vector $\mathbf{a}_{\mathrm{gc}}$ to minimize the thrust acceleration from the SEP system. Inserting this result into Eq. (23) yields

$$a_T^2(\alpha) = a_{\mathrm{gc}}^2 - 2a_{\mathrm{gc}}a_s(0)\cos(\tilde{\theta} - \theta) + a_s^2(0) \tag{27}$$

Equation (27) can be minimized numerically for $\alpha^*(0)$, for example, by using Mathematica® and specifying the bounds for $\alpha \in [0, \pi/2]$.

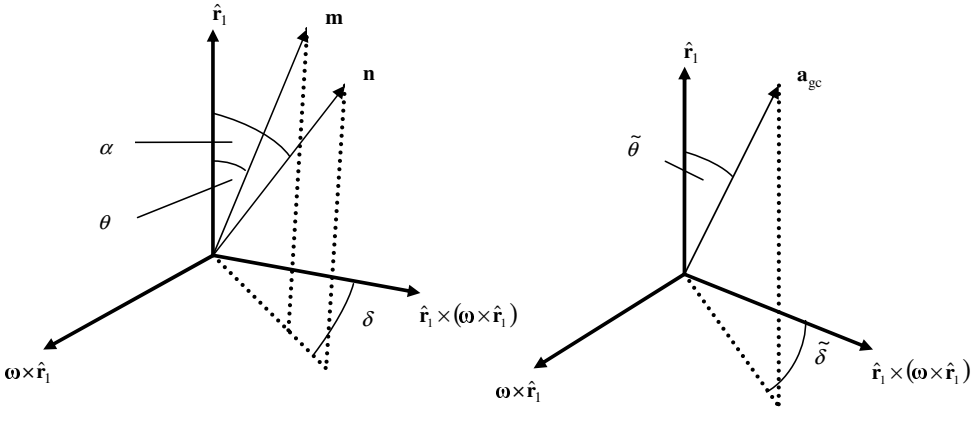

Fig. 4 Definition of the cone and clock angles for vectors n, m, and $\mathbf{a}_{\mathrm{gc}}$ in frame F_b.

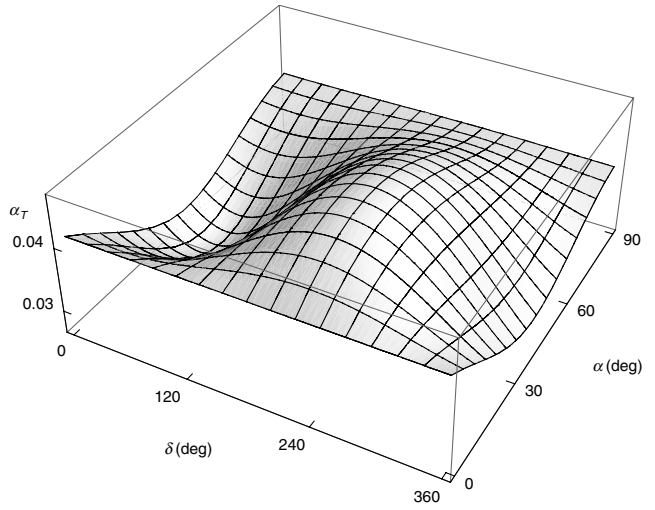

Fig. 5 Required low-thrust acceleration from the SEP at $\mathbf{r}_0 = [1.005 \quad 0.005 \quad 0.005]^T$ as a function of the sail pitch angle α and sail clock angle δ for a sail with $\beta_0 = 0.03$. Minimum $a_T = 0.0269$ at optimal angles $(\alpha^*(0), \delta^*(0)) = (40.23 \text{ deg}, 39.46 \text{ deg})$.

To show the feasibility of the hybrid sail for the practical missions to be discussed in Sec. V, we will now only consider the analysis in the xz plane ($\delta^* = \tilde{\delta} = 0$ if $a_3 > 0$ and $\delta^* = \tilde{\delta} = \pi$ if $a_3 < 0$). Figure 6 shows families of thrust acceleration contours near the Earth in the case of pure SEP and a hybrid sail. The shaded area shows the region in which the pure sail cannot be placed as the SRP force direction is constrained by the maximum cone angle ($\theta \leq \theta_{\max}$) due to the sail film partial reflectivity. The benefit of the hybrid sail over the pure sail is clear. The pure sail can be placed in the shaded region by combining it with an electric thruster, because the thrust vector from the SEP system of a hybrid sail can be oriented in any direction. Also, the benefit of the hybrid sail over pure SEP is clear, because a larger volume of space is available for the artificial equilibrium solutions around L_2, and the displaced equilibrium solutions toward Earth near L_1 exist with the same low-thrust acceleration value ($a_T = 0.02$). This is due to part of the total acceleration, to cancel the gravitational and centrifugal forces of the two primary bodies, being available from the solar sail. In general, the addition of a small SEP system to a solar sail allows the hybrid sail to be in equilibrium closer to the Earth and in volumes of space inaccessible to a pure sail system.

In Fig. 6, we can compare the electric thruster acceleration contours in the case of the pure SEP and the hybrid sail system. The electric thruster acceleration contour of value $a_T = 0.03$ about the Earth in the case of the hybrid system is not symmetric. This depends upon where the hybrid sail can or cannot use SRP effectively. However, the electric thruster acceleration contours of values $|\nabla U| = 0.03$ around the Earth for pure SEP are symmetric due to the near symmetric three-body potential at the Earth. From Earth toward L_1 along the x axis, and also in regions beyond L_2, the acceleration contours of the hybrid sail and the pure SEP are identical because at these locations the hybrid sail cannot use SRP effectively. Here the sail pitch angle becomes approximately 90 deg to minimize the required thrust acceleration from the SEP system. At these locations, the hybrid sail will not be of use as compared with a pure SEP system.

B. Equilibria Options During Mission Life

The hybrid sail is a variable mass system, unlike a pure sail, which is a constant mass system. As the SEP system consumes propellant, the magnitude of the SRP acceleration continuously increases with time due to the decrease of the hybrid sail mass m. In principle, the thrust magnitude needed from the SEP system should decrease with mission lifetime. There are two options to keep the hybrid sail at an AEP $\mathbf{r}_0$ during its mission life.

1. *Option 1*

In option 1, a_T can be minimized at $t = 0$ or for initial mass $m = m_0$ as in the previous section, and the hybrid sail can be maintained at this optimum fixed attitude $(\alpha^*(0), \delta^*(0))$ during the whole mission lifetime. Because of the increase of the SRP acceleration a_s, the thrust from the SEP system should be adjusted in magnitude (throttled) and its direction trimmed at each instant to ensure that the equilibrium condition is satisfied. The algorithm works as follows:

1) At $t = 0$, $m = m_0$, choose the appropriate β_0 so that the total sail area $A_T = m_0\beta_0/\sigma^*$.

2) In the xz plane, choose an AEP $\mathbf{r}_0$ that in turn determines the desired acceleration vector $\mathbf{a}_{gc}$. Calculate the cone angle $\tilde{\theta}$ using Eq. (21). However, in the xz plane, $a_2 = 0$. And so from

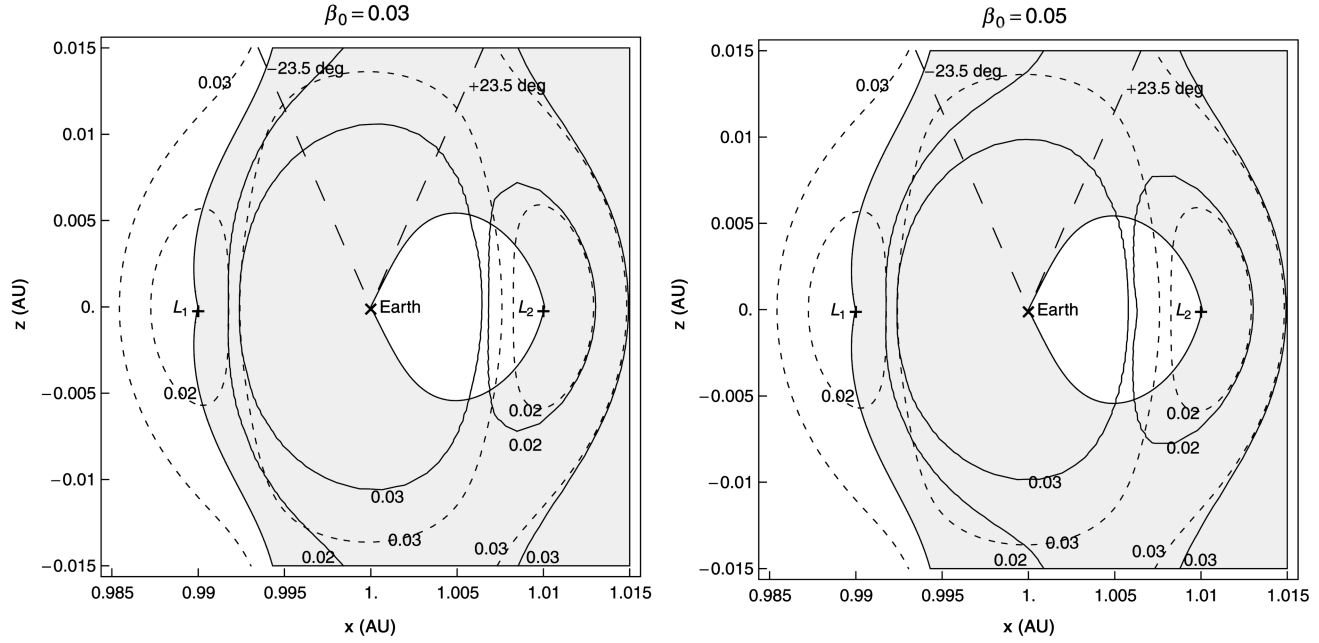

Fig. 6 Thrust acceleration contours a_T in the xz plane. Values 0.02 and 0.03 are shown by dotted lines for the pure SEP system and shown by solid lines for the hybrid sail. ∓ 23.5 deg are the angles of polar axis of Earth (dashed lines) with respect to the normal to the ecliptic plane at the summer and winter solstices.

Eq. (22), $\tilde{\delta} = 0$ or π, which implies the clock angle $\delta^*(0) = 0$ or π.

3) Minimize a_T given in Eq. (27) for a hybrid sail of mass m_0, determine the optimum sail pitch angle $\alpha^*(0)$, and keep it fixed for mission lifetime τ_m, that is, $\alpha^*(t) = \alpha^*(0)$ for $0 \le t \le \tau_m$. The normal to the hybrid sail $\mathbf{n}$ and unit vector $\mathbf{m}$ along the SRP force given in Eq. (20) become

$$\begin{aligned} \mathbf{n}^b &= \begin{bmatrix} \cos\alpha^*(0) & 0 & \pm\sin\alpha^*(0) \end{bmatrix}^T \\ \mathbf{m}^b &= \begin{bmatrix} \cos\theta^*(0) & 0 & \pm\sin\theta^*(0) \end{bmatrix}^T \end{aligned} \tag{28}$$

where $\theta^*(0)$ is calculated using Eq. (9).

4) Calculate the SRP acceleration a_s and SEP acceleration a_T for a hybrid sail of mass m from Eqs. (7) and (23), respectively, at the optimum sail pitch angle and clock angle $\delta^*(t) = \tilde{\delta} = 0(\pi)$.

5) Calculate the consumed propellant mass $m_{\text{prop}}(t)$ up to time t:

$$m_{\text{prop}}(t) = m_0\left(1 - \exp\left(-\frac{1}{I_{\text{sp}} g_0}\int_0^t \acute{a}_T \, \mathrm{d}t\right)\right) \tag{29}$$

so that the instantaneous mass of the hybrid sail $m = m_0 - m_{\text{prop}}$.

6) Calculate the electric thruster direction at time t:

$$\mathbf{u}^b = \begin{bmatrix} u_1 & 0 & u_3 \end{bmatrix}^T = (1/a_T)[\mathbf{a}_{\text{gc}}^b - a_s \mathbf{m}^b] \tag{30}$$

7) $t = t + \triangle t$. If $t < \tau_m$ go to step 4; otherwise, the calculation is over.

2. Option 2

In option 2, the optimum sail pitch angle $\alpha^*(t)$ at each instant t is determined using the instantaneous mass m during the mission lifetime, instead of fixing it at $\alpha^*(0)$. In this case, both $\mathbf{n}$ and $\mathbf{u}$ will be varied to keep the hybrid sail at an artificial equilibrium point $\mathbf{r}_0$. The algorithm in this case works similarly to option 1 except steps 3 and 7 should be replaced accordingly:

3) Minimize a_T given in Eq. (23) with $\delta^*(t) = \tilde{\delta} = 0$ or π and determine the optimum sail pitch angle $\alpha^*(t)$ using the instantaneous mass m of the hybrid sail. The unit vectors $\mathbf{n}^b$ and so $\mathbf{m}^b$ in this case will vary with time as

$$\begin{aligned} \mathbf{n}^b &= \begin{bmatrix} \cos\alpha^*(t) & 0 & \pm\sin\alpha^*(t) \end{bmatrix}^T \\ \mathbf{m}^b &= \begin{bmatrix} \cos\theta^*(t) & 0 & \pm\sin\theta^*(t) \end{bmatrix}^T \end{aligned} \tag{31}$$

where $\theta^*(t)$ is calculated using $\alpha^*(t)$.

7) $t = t + \triangle t$. If $t < \tau_m$ go to step 3; otherwise, the calculation is over.

IV. Linear Stability Analysis for the Hybrid Sail

A. Linearized System

To determine the local stability property of an AEP $\mathbf{r}_0$, the variational equations in the vicinity of an equilibrium point are derived. Such linearized variational equations are obtained by replacing the nonlinear system Eq. (15) by a linear system around the equilibrium point $\mathbf{r}_0$. Using the transformation $\mathbf{r} = \mathbf{r}_0 + \delta\mathbf{r}$ for linearization (in the xz plane) and assuming the attitude of the hybrid sail $\mathbf{n}^a$ and thruster pointing of the SEP system $\mathbf{u}^a$ are not perturbed so as to restrict the stability analysis in the sense of Lyapunov, Eq. (15) can be rewritten in the following form:

$$\begin{aligned} &\frac{\mathrm{d}^2\delta\mathbf{r}}{\mathrm{d}t^2} + 2\boldsymbol{\omega} \times \frac{\mathrm{d}\delta\mathbf{r}}{\mathrm{d}t} + \nabla U(\mathbf{r}_0 + \delta\mathbf{r}) \\ &\quad = \mathbf{a}_S(\mathbf{r}_0 + \delta\mathbf{r}, \mathbf{n}^a) + \mathbf{a}_{\text{SEP}}(\mathbf{r}_0 + \delta\mathbf{r}, \mathbf{u}^a) \end{aligned} \tag{32}$$

The gradient of the potential and the acceleration vectors due to SRP and SEP can be expanded in a Taylor series about the equilibrium point $\mathbf{r}_0$ to a first order as

$$\begin{aligned} \nabla U(\mathbf{r}_0 + \delta\mathbf{r}) &= \nabla U(\mathbf{r}_0) + \left[\frac{\partial \nabla U}{\partial \mathbf{r}}\right]_{\mathbf{r}_0} \delta\mathbf{r} + O(|\delta\mathbf{r}|^2) \\ \mathbf{a}_S(\mathbf{r}_0 + \delta\mathbf{r}, \mathbf{n}^a) &= \mathbf{a}_S(\mathbf{r}_0) + \left[\frac{\partial \mathbf{a}_S(\mathbf{r})}{\partial \mathbf{r}}\right]_{(\mathbf{r}_0, \mathbf{n}^a)} \delta\mathbf{r} + O(|\delta\mathbf{r}|^2) \\ \mathbf{a}_{\text{SEP}}(\mathbf{r}_0 + \delta\mathbf{r}, \mathbf{u}^a) &= \mathbf{a}_{\text{SEP}}(\mathbf{r}_0) + \left[\frac{\partial \mathbf{a}_{\text{SEP}}}{\partial \mathbf{r}}\right]_{(\mathbf{r}_0, \mathbf{u}^a)} \delta\mathbf{r} + O(|\delta\mathbf{r}|^2) \end{aligned} \tag{33}$$

Assuming the acceleration $\mathbf{a}_{\text{SEP}}$ is fixed with respect to the perturbation $\delta\mathbf{r}$, we have

$$\left[\frac{\partial \mathbf{a}_{\text{SEP}}}{\partial \mathbf{r}}\right]_{\mathbf{r}_0} = 0 \tag{34}$$

Substituting Eqs. (33) and (34) into Eq. (32) and using the artificial equilibrium condition of Eq. (16), the linear variational equation around an AEP $\mathbf{r}_0$ is obtained:

$$\frac{\mathrm{d}^2\delta\mathbf{r}}{\mathrm{d}t^2} + 2\boldsymbol{\omega} \times \frac{\mathrm{d}\delta\mathbf{r}}{\mathrm{d}t} - K\delta\mathbf{r} = 0 \tag{35}$$

where

$$K = -\left[\frac{\partial \nabla U}{\partial \mathbf{r}}\right]_{\mathbf{r}_0} + \left[\frac{\partial \mathbf{a}_S(\mathbf{r})}{\partial \mathbf{r}}\right]_{(\mathbf{r}_0, \mathbf{n}^a)} \tag{36}$$

For an artificial equilibrium point $\mathbf{r}_0$ in the xz plane, the explicit expression for K is given in the Appendix.

By letting $\mathbf{X} = (\delta\mathbf{r}, \delta\dot{\mathbf{r}})^T$, the linear system is $\dot{\mathbf{X}} = A(t)\mathbf{X}$. The Jacobian matrix $A(t)$ in the neighborhood of $\mathbf{r}_0$ is given by

$$A(t) = \begin{pmatrix} 0 & I \\ K & \Omega \end{pmatrix}, \qquad \Omega = \begin{pmatrix} 0 & 2 & 0 \\ -2 & 0 & 0 \\ 0 & 0 & 0 \end{pmatrix} \tag{37}$$

The Jacobian matrix is constant when the dynamics of the pure sail are linearized in the CRTBP. However, the linearization for a hybrid sail in the CRTBP is a time-varying system as the matrix K given in Eq. (36) contains mass (time) varying parameters. The necessary condition for asymptotically stability of a linear time-varying system is that for any $t > t_0$ [17]

$$\int_{t_0}^{t} \mathrm{tr}A(\tau)\,\mathrm{d}\tau \to -\infty \quad \text{as} \quad t \to \infty \tag{38}$$

where $\mathrm{tr}A(\tau)$ is the trace of $A(t)$. Because, for the hybrid sail,

$$\int_{t_0}^{t} \mathrm{tr}A(\tau)\,\mathrm{d}\tau = 0 \tag{39}$$

it can be concluded that the linear time-varying system of the hybrid sail is not asymptotically stable, as is expected because there is no natural dissipation. One approach to investigate the instability of slowly time-varying linear systems is to employ a freezing-time method [18]. In this approach, the time-varying parameters (e.g., mass m for a hybrid system) are fixed at their current values during each instant of time $t = t_0, t_1, t_2, \ldots, \tau_m$ and the Jacobian matrix $A(t_i)$ will be treated as constant for each interval t_i to t_{i+1}. Then, the eigenvalues of the constant matrix $A(t_i)$ resulting from its characteristic equation are examined for instability. The instability properties of the time-varying system are the same as those of the frozen-time system provided that the eigenvalues of $A(t)$ are bounded away from the imaginary axis for all $t \ge 0$ (i.e., eigenvalues do not cross the imaginary axis) and if $sup_{t\ge 0}\|\dot{A}(t)\|$ (i.e., the norm of the time derivative of matrix $A(t)$) is sufficiently small [18].

B. Stability Analysis at $t_0 = 0$

To determine the stability of the linear system $\dot{\mathbf{X}} = A(t_0)\mathbf{X}$, the Jacobian matrix $A(t)$ time dependence is frozen at $t_0 = 0$ by substituting $m = m_0$ in the matrix K of Eq. (36), so that K may be written as

$$K(t_0) = \begin{pmatrix} k_1 & 0 & k_3 \\ 0 & k_5 & 0 \\ k_7 & 0 & k_9 \end{pmatrix} \tag{40}$$

The characteristic equation of $A(t_0)$ in λ is given by

$$|A(t_0) - \lambda I_6| = \lambda^6 + p_2\lambda^4 + p_1\lambda^2 + p_0 = 0 \tag{41}$$

where

$$p_2 = 4 - k_1 - k_5 - k_9 \tag{42}$$

$$p_1 = k_1k_5 - k_3k_7 - 4k_9 + k_1k_9 + k_5k_9 \tag{43}$$

$$p_0 = k_3k_5k_7 - k_1k_5k_9 \tag{44}$$

If we define $\xi = \lambda^2$, then the characteristic equation becomes cubic in ξ such that

$$\xi^3 + p_2\xi^2 + p_1\xi + p_0 = 0 \tag{45}$$

The discriminant of the cubic Eq. (45) can be then defined as

$$D = 4p_0p_2^3 - p_1^2p_2^2 + 4p_1^3 - 18p_0p_1p_2 + 27p_0^2 \tag{46}$$

The roots of the cubic Eq. (45) in ξ are real if the discriminant $D \leq 0$ or, alternatively, one real root and a pair of complex conjugate roots if $D > 0$. However, if all the roots of the cubic equation are real, that is, $D \leq 0$, then by *Descartes's rule of signs* [19], the number of positive real roots (including multiplicity) is equal to the number of sign changes of the sequence p_0, p_1, and p_2 in Eq. (45).

The nature of the artificial equilibria (in the xz plane) for the sun–Earth CRTBP, in which the third body is a hybrid sail, is shown in Fig. 7. We label the regions as follows:

Region I: If the discriminant $D < 0$ and $p_0 > 0$, $p_1 > 0$, and $p_2 > 0$, then by Descartes's rule of signs, with no sign change of the coefficient sequence of the cubic equation, all the roots of Eq. (45) are negative. Therefore, the spectrum of the Jacobian $A(t_0)$ consists of centers crossed with saddles given by

$$\{\pm i\lambda_1, \pm i\lambda_2, \pm i\lambda_3\} \qquad \text{region I marginally stable}$$

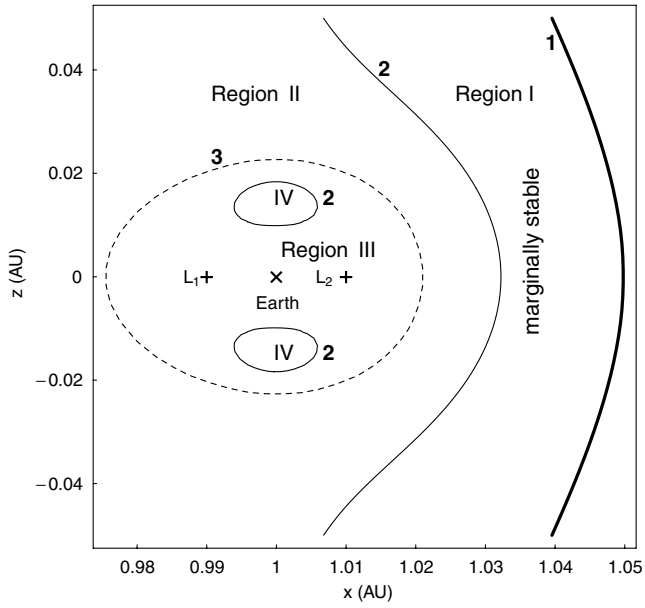

Fig. 7 Regions I–IV in the sun–Earth three-body system are classified according to the stability of artificial equilibria for a hybrid sail. Numbers 1, 2, and 3 represent the contours of $D = 0$, $p_0 = 0$, and $p_1 = 0$, respectively.

Regions II and III: If in region II the discriminant $D < 0$ and $p_0 < 0$, $p_1 > 0$, and $p_2 > 0$, or in region III the discriminant $D < 0$ and $p_0 < 0$, $p_1 < 0$, and $p_2 > 0$, then by Descartes's rule of signs, with one sign change of the coefficient sequence of the cubic equation, the spectrum of the Jacobian is centers crossed with saddles:

$$\{\pm i\lambda_1, \pm i\lambda_2, \pm\lambda_{r_1}\} \qquad \text{regions II and III unstable}$$

Region IV: If the discriminant $D < 0$ and $p_0 > 0$, $p_1 < 0$, and $p_2 > 0$, then by Descartes's rule of signs, with two sign changes of the coefficient sequence of the cubic Eq. (45), the spectrum is

$$\{\pm i\lambda_1, \pm\lambda_{r_1}, \pm\lambda_{r_2}\} \qquad \text{region IV unstable}$$

The hybrid sail in region I does not use SRP as the pitch angle $\alpha^*(0)$ becomes approximately/or equal to 90 deg to minimize the thrust acceleration a_T from the SEP system. Therefore, in this region the hybrid sail acts as a pure SEP system and the marginally stable region (centers) of the pure SEP system are recovered [12].

During the mission life at an artificial equilibria location $\mathbf{r}_0$, the mass m of the hybrid sail changes according to Eq. (29). Hence, the matrix $A(t)$ and its eigenvalues also change with m. Simulations run for different artificial equilibria in regions II–IV with corresponding mass variation show very slow variation and no sign change in the roots of the cubic Eq. (45) during the mission life. Thus, no eigenvalues cross the imaginary axis and the small parameter variations in $A(t)$ during the mission life imply the instability of regions II–IV.

V. Evaluation of Hybrid Sail Performance

This section compares the sizing of a hybrid sail, a pure SEP system, and a pure sail system for a polar (Earth) observer mission. In the polar observer mission, AEPs along the polar axis, high above the L_1 side of the Earth, are selected in the sun–Earth system. Such equilibrium locations have been proposed by Crison and Dittberner [8] and McInnes et al. [20] in the case of a pure sail for continual, low-resolution imaging of high-latitude regions of the Earth and for polar telecommunication services at L_2 [10].

The magnitude of the required acceleration a_{gc} for an AEP along the polar axis is shown by the dotted lines in Fig. 8. It can be seen that a_{gc} has a minimum value along the polar axis due to the sun–Earth three-body dynamics. To generate an AEP, the pure SEP system alone provides the acceleration a_{gc}. For the hybrid sail, the thruster system provides less acceleration $a_T(\alpha^*(0))$, shown by the solid lines in Fig. 8, because part of the acceleration is provided by the SRP to achieve a_{gc}.

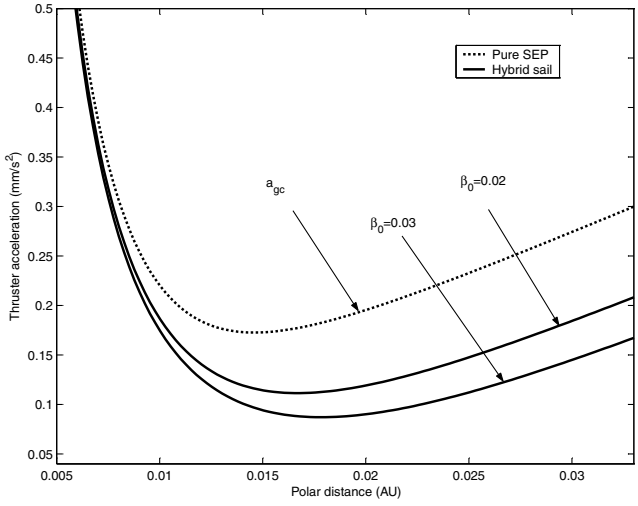

Fig. 8 Thrust acceleration magnitude required from the pure SEP and hybrid sail (at $t = 0$) at artificial equilibrium points above L_1 along the Earth's polar axis (North Pole at the summer solstice).

The initial (wet) mass for each propulsion system is calculated to position a spacecraft on an AEP with a fixed payload mass $m_{\rm pl}$ and fixed mission life τ_m. The total payload mass (including a small optical imager and spacecraft bus) of 100 kg is assumed for the polar observer mission. The pure sail is a propellantless system, unlike pure SEP and the hybrid sail, and the pure sail mission life is limited only by the sail film. Hence, for the pure sail system, only the payload mass $m_{\rm pl}$ is fixed. Some near-term pure sail missions are envisaged with a sail lifetime of at least 5 years [21].

A. Pure Sail

For a pure sail, the total mass m_0 can be decomposed into the sail assembly mass m_S (sail film, booms, and deployment module) and the payload mass $m_{\rm pl}$. The sail assembly mass m_S is usually written in terms of the sail area and sail assembly loading σ_S (defined as mass per unit area of the sail assembly), a key technology parameter that is a measure of the sail film thickness and lightness of the booms and deployment module. For a fixed $m_{\rm pl}$ and σ_S as given parameters, the initial mass can be calculated for a given equilibrium location $\mathbf{r}_0$:

$$m_0 = m_{\rm pl} + m_S = m_{\rm pl} + \sigma_S\left[\frac{m_{\rm pl}}{\sigma_T - \sigma_S}\right] \tag{47}$$

where $\sigma_T = m_0/A_s$ is the total (pure) sail loading. It can be calculated from the appropriate sail lightness number, which is uniquely determined by the chosen equilibria location $\mathbf{r}_0$ and the sail film reflectivity $\tilde{r}_S$ [22].

B. Pure SEP

The polar observer mission is a long-term and large ΔV mission. To reduce m_0 for a given $m_{\rm pl}$, in the case of pure SEP and the hybrid sail, electric thruster selection should be made to reduce the propellant mass $m_{\rm prop}$ and the electric propulsion inert mass. Ion thrusters, among various kinds of electric propulsion systems, are well suited because of their potential for providing high $I_{\rm sp} \approx 3200$ s (which reduces the propellant requirement), high efficiency, and a higher total impulse [23]. Higher efficiency for a given $I_{\rm sp}$ and thrust level reduces the input power of the SEP system, whereas a higher total impulse reduces the number of thrusters and thus also the inert mass of the SEP system. For a pure SEP system with TFSC technology as a power source, the initial mass m_0 breakdown can be written as

$$m_0 = m_{\rm pl} + m_{\rm Tank} + n_{\rm Th} \cdot m_{\rm inert} + m_{\rm prop} + m_{\rm TF} \tag{48}$$

where $m_{\rm Tank}$ is the (empty) propellant tank mass, $m_{\rm prop}$ is the propellant mass, $m_{\rm TF}$ is the TFSC mass, and $m_{\rm inert}$ is the inert mass of SEP system including the mass of the thruster, the power processor unit (PPU), the thermal system for the PPU, the digital control and interface unit, and the cabling/propellant feeding system. $n_{\rm Th}$ is the number of thrusters. Two thrusters are assumed in series, each with an operating life of 2.5 years. To maintain the artificial equilibria $\mathbf{r}_0$, the constant acceleration $a_{\rm gc}(\mathbf{r}_0)$ should be provided by the pure SEP system during mission life τ_m; thus, the propellant mass consumed $m_{\rm prop}$ is given by

$$m_{\rm prop} = m_0\left(1 - \exp\left(\frac{-\acute{a}_{\rm gc}\tau_m}{I_{\rm sp}g_0}\right)\right) \tag{49}$$

In the case of ion thrusters, the approximate relations in Eq. (48) are given by

$$m_{\rm Tank} = 0.1 m_{\rm prop} \qquad m_{\rm inert} = k_e P_{e,\max} \qquad m_{\rm TF} = \sigma_{\rm TF} A_{\rm TF} \tag{50}$$

The reasonable assumption is made that the mass of the propellant tank $m_{\rm Tank}$ is 10% of the propellant mass [24]. The specific mass k_e is assumed to be 20 kg/kW (as for the NASA Solar Electric Propulsion Technology Application Readiness class engine [25]). The areal density $\sigma_{\rm TF}$ of the TFSC is assumed to be 100 g/m^2 [14]. The thin-film solar cell area $A_{\rm TF}$ is selected by using the maximum power level required $P_{e,\max}$ (or maximum thrust $T_{\max}$), the solar flux W at the AEP $\mathbf{r}_0$, and the efficiency $\eta_{\rm TF}$ (i.e., converting solar energy into electrical energy):

$$A_{\rm TF} = \frac{P_{e,\max}}{W\eta_{\rm TF}} \tag{51}$$

In Eq. (51), the TFSC area is assumed to be pointed at the sun while the ion thruster is firing in the desired direction to maintain the artificial equilibrium $\mathbf{r}_0$. Although TFSC technology gives larger $A_{\rm TF}$ as compared with wafer-based technology for a required $P_{e,\max}$, due to its low efficiency $\eta_{\rm TF} = 0.05$, it results in a lower mass $m_{\rm TF}$ due to the small value of $\sigma_{\rm TF}$. If $\eta_e = 0.7$ [26] is the efficiency of converting electrical energy into constant exhaust velocity $v_e = I_{\rm sp}g_0$, then

$$P_{e,\max} = \frac{T_{\max}v_e}{2\eta_e} = \frac{m_0\acute{a}_{\rm gc}I_{\rm sp}g_0}{2\eta_e} \tag{52}$$

The initial (wet) mass m_0 for a pure SEP system then can be written in terms of $m_{\rm pl}$ and τ_m by substituting Eqs. (49–52) into Eq. (48):

$$m_0 = \frac{m_{\rm pl}}{1 - 1.1\left(1 - \exp\left(\frac{-\acute{a}_{\rm gc}\tau_m}{I_{\rm sp}g_0}\right)\right) - \frac{\acute{a}_{\rm gc}I_{\rm sp}g_0}{2\eta_e}\left(k_e n_{\rm Th} + \frac{\sigma_{\rm TF}}{W\eta_{\rm TF}}\right)} \tag{53}$$

C. Hybrid Sail

The initial mass breakdown for a hybrid sail is assumed as follows:

$$m_0 = m_{\rm pl} + m_{\rm Tank} + n_{\rm Th}(m_{\rm inert} + m_{\rm gimbal}) + m_{\rm prop} + m_{\rm TF} + m_S \tag{54}$$

Here the gimbal mass $m_{\rm gimbal}$ for each engine is assumed to be 30% of the inert mass of the thruster system $m_{\rm inert}$ [24]. A gimbal is required to actuate the thruster relative to the sail assembly to maintain equilibrium. With a given m_0, the propellant mass $m_{\rm prop}$ required to maintain the artificial equilibrium for a mission life τ_m can be calculated using the algorithms described in Sec. III.B. In Eq. (54), for $m_{\rm Tank}$, $m_{\rm inert}$ and $m_{\rm TF}$, the same approximate relations for the pure SEP system given in Eq. (50) are assumed. However, with a given m_0, we replace the maximum thrust level by $T_{\max} = m_0 a_T(\alpha^*(0))$ in Eq. (52) and, moreover, divide Eq. (51) by $\cos(\alpha^*(0))$ to calculate $m_{\rm inert}$ and $m_{\rm TF}$, respectively, because the TFSC is attached to the sail and so is not sun pointing. Also, with a given m_0, the sail mass m_S in Eq. (54) is given by

$$m_S = \sigma_S A_T = \sigma_S(m_0\beta_0/\sigma^*) \tag{55}$$

In summary, for a given β_0, τ_m, σ_S, and an initial guess m_0, the payload mass $m_{\rm pl}$ can be calculated using Eq. (54). A simple shooting method is used to determine m_0 for different artificial equilibria along the polar axis so that the payload mass $m_{\rm pl}$ becomes 100 kg.

Figure 9 shows that the minimum initial mass m_0 along the polar axis is located at 0.0145 astronomical units (AU) for a pure SEP, at 0.025 AU for a pure sail with sail film reflectivity $\tilde{r}_S = 0.9$, and at 0.0183 AU for a hybrid sail with $\beta_0 = 0.03$. For the pure SEP system, the minimum m_0 at 0.0145 AU is due to the minimum $a_{\rm gc}$ at 0.0145 AU (see Fig. 8). For a pure sail, the minimum is shifted to 0.025 AU due to the variation of SRP acceleration with α. For a hybrid sail, the location of the minimum m_0 depends upon the minimum location of $a_T(\alpha^*(0))$ (see Figs. 8 and 9). Figures 9a–9c also show the dependence of m_0 for the pure sail and hybrid sail systems with the variation of the sail assembly loading. The vertical line shows that the pure sail cannot be placed along the polar axis below 0.015 AU. The sail assembly loading of 15, 10, and 5 g/m^2 may be assumed for near-, mid, and far-term sails [24]. Figure 9 shows that, for a near-term sail assembly loading of 13.75 g/m^2, the minimum initial mass m_0 for a pure SEP (with a maximum power level of 1.5 kW) and a pure sail (with a sail length of 170 m) becomes equal to 500 kg, and the hybrid sail clearly has a lower initial mass of 365 kg (a sail length of 85 m and a maximum power level of 715 W) at an optimum distance of 0.0183 AU and thus a lower launch mass and higher resolution for imaging than the pure sail. Figure 9c shows that, for a far-term sail assembly loading, that is, 5 g/m^2, the hybrid sail has a significant improvement in payload fraction below

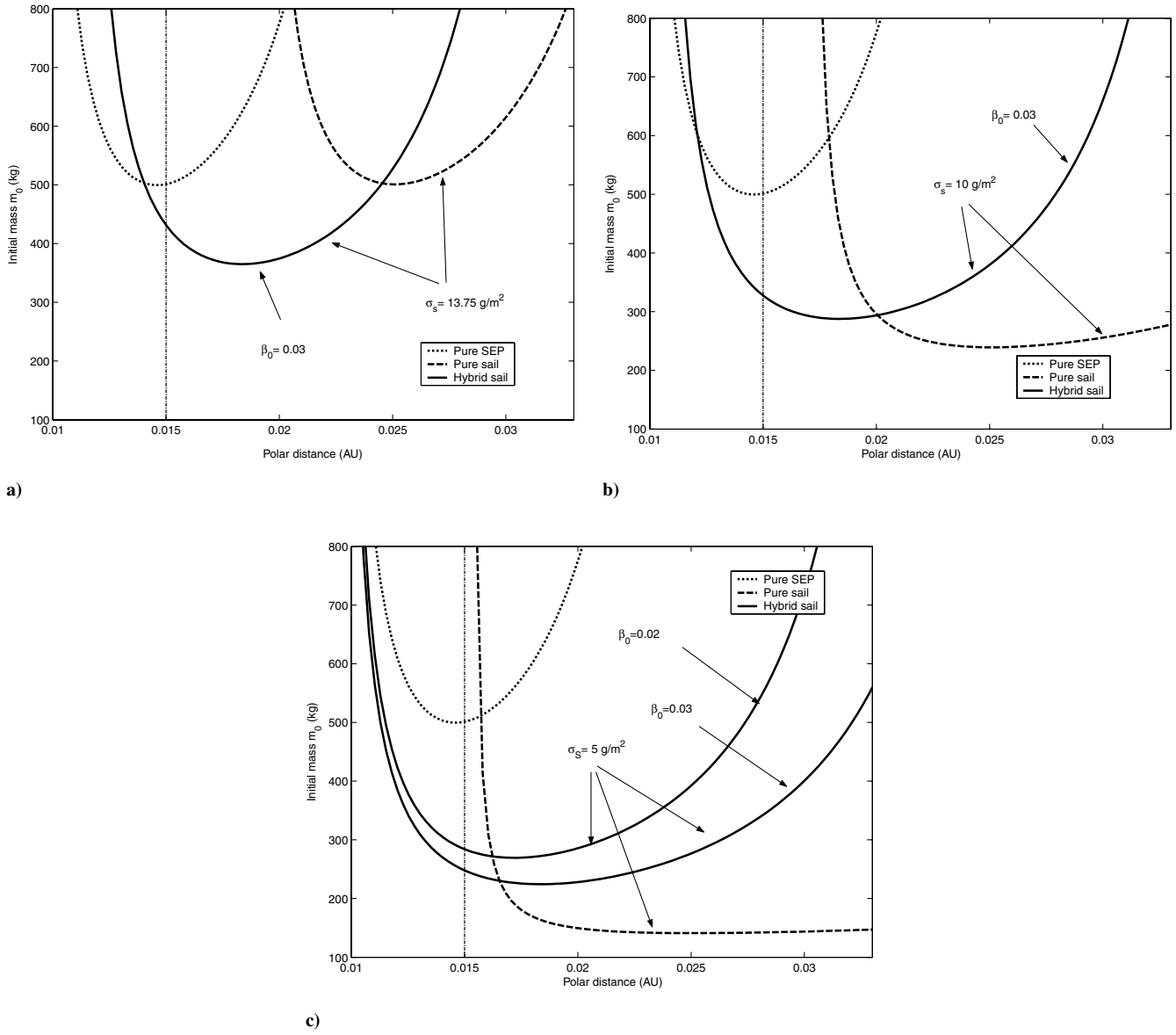

Fig. 9 Spacecraft initial (wet) mass required for an AEP for a 100-kg payload for a polar observer mission (above L_1). Five-year mission lifetime is considered for a pure SEP and hybrid sail. Initial mass variation for a pure and hybrid sail with sail assembly loading equal to a) 13.75 g/m^2, b) 10 g/m^2, and c) 5 g/m^2 are also shown.

0.015 AU along the polar axis as compared with the pure SEP and also a higher resolution for imaging than a pure sail.

Table 1 shows the initial mass breakdown with a midterm sail assembly loading for station keeping a 100-kg payload mass at a polar distance of 0.01831 AU (see Fig. 9b). The hybrid sail total initial mass m_0 at this AEP is less than that of the pure SEP and pure sail systems. The hybrid sail total mass is less than the total mass of the pure SEP as the savings in propellant mass and inert mass of the thruster system for the hybrid sail, totaling 389 kg, is greater than the additional penalty of the sail assembly mass $m_S = 56.5$ kg compared

Table 1 Mass breakdown for three different propulsion systems for a spacecraft stationed at a polar distance 0.01831 AU along the polar axis above L_1. A fixed payload mass and fixed mission life of 5 years is assumed in the case of pure SEP and hybrid sail

Subsystem	Pure sail[a] ; mass budget, kg	Pure SEP; mass budget, kg	Hybrid sail[a] ; mass budget, kg
m_{pl}	100	100	100
m_{prop}	——	376	92
m_{inert}(1st thruster)	——	51.5[b]	11.3[b]
m_{gimbal}	——	——	3.4
m_{Tank}	——	37.5	9.2
m_{TF}	——	4.5	1.2
m_{inert}(2nd thruster)	——	51.5	14.7[c]
m_S	360	——	56.5
m_0 (total initial mass)	460	621	288

[a]Pure sail length = 190 m and hybrid sail length = 75 m; sail assembly loading $\sigma S = 10$ g/m^2.
[b]$P_{e,\max} = 564$ W for hybrid sail, $P_{e,\max} = 2.58$ kW for pure SEP.
[c]Also includes gimbal mass.

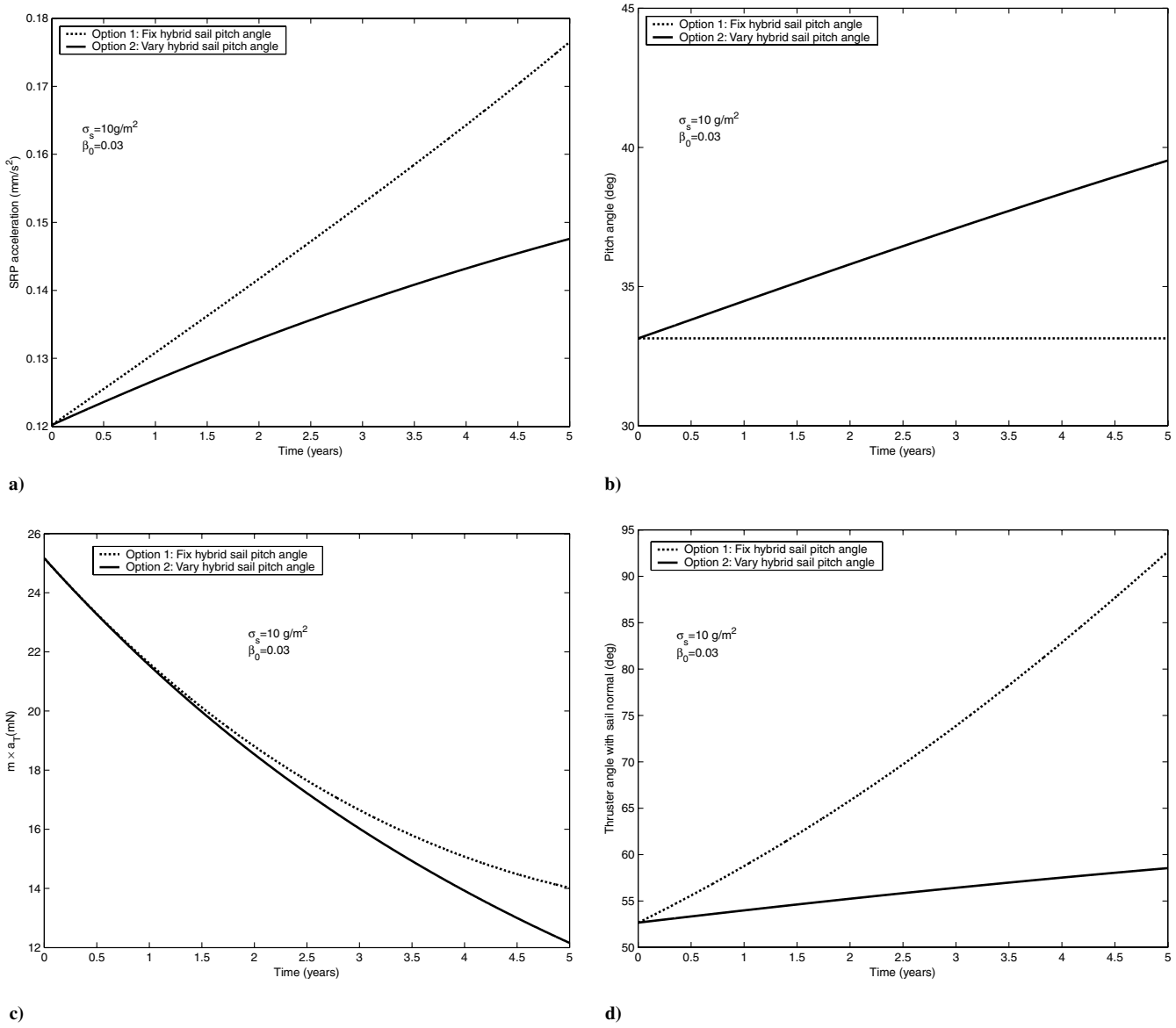

Fig. 10 Hybrid sail during mission life stationed at polar distance 0.01831 AU along the polar axis above L_1: a) SRP acceleration magnitude, b) pitch angle, c) ion thruster force, and d) ion thruster firing angle with regard to sail normal.

with the pure SEP. The smaller inert mass of the thruster system for the hybrid sail is due to the lower maximum power required as compared with the maximum power for a pure SEP thruster system. The hybrid sail total mass is less than the total mass of the pure sail as the savings from the sail mass for the hybrid sail, by reducing the sail length, is greater than the penalty of the propellant and inert mass of the thruster system needed for the hybrid sail. Table 1 shows that the mass of the TFSC area is small compared with the inert mass, tank, and propellant of the SEP system [14].

Figure 10 shows the hybrid sail parameter variation during the mission life when it is in a static equilibrium with either of the two equilibria strategies (options 1 and 2). Figure 10a shows the increase of SRP magnitude a_s due to the decrease of mass m during the mission life. For option 2, there is a slow variation in a_s due to the increase of the hybrid sail pitch angle $\alpha^*(t)$ as compared with its fixed pitch angle $\alpha^*(0)$ for option 1 (see Fig. 9b). Figures 10c and 10d show the required force and orientation of the SEP thruster system to maintain the equilibrium condition. Although the same orientation, 52.66 deg for this AEP, is required at the start of the mission in both options, there is less variation in the orientation of the ion thruster system relative to the sail normal for option 2. Option 2 is better than option 1, as the thruster plume does not interact with the sail film during the whole mission life (see Fig. 10d). Moreover, in option 2, less thrust is required during the whole mission life (see Fig. 10c) with fixed I_{sp}, which suggests less total propellant mass consumption and hence less total initial mass m_0. However, for both options, the ion thruster system must have the capability of throttling down, and a gimbal system is required to maintain equilibrium.

VI. Conclusions

In this paper, a new concept to generate artificial equilibrium points by using a hybrid solar sail in the circular restricted three-body problem has been analyzed. The key idea is that the required acceleration vector to keep the hybrid sail at an artificial equilibrium point is achieved by the vector sum of the solar radiation pressure acceleration and the solar electric propulsion acceleration vectors. We cast the problem to minimize the acceleration from the SEP system of the hybrid sail for a given sail lightness number. It is shown that the hybrid sail clock angle should be aligned with the clock angle of the required acceleration vector to minimize acceleration from the SEP system. Finally, the minimization problem for equilibrium reduces to numerically determining the optimum hybrid sail pitch angle. A linear stability analysis shows that the artificial equilibrium points for the hybrid sail are unstable in general, apart from some regions in which the equilibria are marginally stable. Moreover, the

time-varying parameter (mass variation) of the hybrid sail does not change the stability properties of the equilibria. It has been shown that the hybrid sail has a potential application of hovering above the L_1 point for real-time, low-resolution images of the poles. The hybrid sail along the polar axis is found to have a lower sail length compared with a pure sail and a lower maximum power level as compared with a pure SEP system. For a near-term sail assembly loading (13.75 g/m^2), the hybrid sail for the polar observer mission clearly demonstrates a greater payload mass fraction. Furthermore, the hybrid sail can be used to obtain higher-resolution images by hovering in a region that is inaccessible for the pure sail.

Appendix: Matrix K

For the matrix $\frac{\partial \nabla U}{\partial \mathbf{r}}$ in Eq. (36) the terms are as follows:

$$\frac{\partial \nabla U}{\partial \mathbf{r}} = \begin{pmatrix} U_{xx} & U_{xy} & U_{xz} \\ U_{yx} & U_{yy} & U_{yz} \\ U_{zx} & U_{zy} & U_{zz} \end{pmatrix} \tag{A1}$$

The acceleration due to solar pressure for a hybrid sail can be rewritten using Eqs. (7) and (12):

$$\mathbf{a}_S = \frac{1}{2}\beta_0 \frac{m_0}{m} \frac{1-\mu}{r_1^4} \psi \mathbf{m}^a \tag{A2}$$

where

$$\psi = [(g^2 - h^2)(\mathbf{r}_1.\mathbf{n})^4 + h^2 r_1^2 (\mathbf{r}_1.\mathbf{n})^2]^{1/2}$$

The partial derivatives of Eq. (A2) can be obtained as

$$\frac{\partial \mathbf{a}_S}{\partial \mathbf{r}} = -2\beta_0 \frac{m_0}{m} \frac{(1-\mu)}{r_1^5} \psi \begin{pmatrix} \frac{(x+\mu)}{r_1} m_x & \frac{y}{r_1} m_x & \frac{z}{r_1} m_x \\ \frac{(x+\mu)}{r_1} m_y & \frac{y}{r_1} m_y & \frac{z}{r_1} m_y \\ \frac{(x+\mu)}{r_1} m_z & \frac{y}{r_1} m_z & \frac{z}{r_1} m_z \end{pmatrix} + \frac{1}{2}\beta_0 \frac{m_0}{m} \frac{(1-\mu)}{r_1^4} \begin{pmatrix} \frac{\partial \psi}{\partial x} m_x & \frac{\partial \psi}{\partial y} m_x & \frac{\partial \psi}{\partial z} m_x \\ \frac{\partial \psi}{\partial x} m_y & \frac{\partial \psi}{\partial y} m_y & \frac{\partial \psi}{\partial z} m_y \\ \frac{\partial \psi}{\partial x} m_z & \frac{\partial \psi}{\partial y} m_z & \frac{\partial \psi}{\partial z} m_z \end{pmatrix} \tag{A3}$$

where

$$\begin{pmatrix} \frac{\partial \psi}{\partial x} \\ \frac{\partial \psi}{\partial y} \\ \frac{\partial \psi}{\partial z} \end{pmatrix} = \frac{2(g^2 - h^2)(\mathbf{r}_1.\mathbf{n})^3 + h^2 r_1^2 (\mathbf{r}_1.\mathbf{n})}{\psi} \begin{pmatrix} n_x \\ n_y \\ n_z \end{pmatrix} + \frac{h^2 (\mathbf{r}_1.\mathbf{n})^2}{\psi} \begin{pmatrix} x+\mu \\ y \\ z \end{pmatrix}$$

and $\mathbf{m}^a = [\,m_x \quad m_y \quad m_z\,]^T$ and $\mathbf{n}^a = [\,n_x \quad n_y \quad n_z\,]^T$ may be calculated as

$$\mathbf{m}^a = \mathbf{C}_{b/a}^T \mathbf{m}^b \qquad \mathbf{n}^a = \mathbf{C}_{b/a}^T \mathbf{n}^b \tag{A4}$$

For an artificial equilibrium point $\mathbf{r}_0$ in the xz plane, $\mathbf{m}^b$ and $\mathbf{n}^b$ are given by Eqs. (28) and (31) for options 1 and 2, respectively. Furthermore, for $\mathbf{r}_0$ in xz plane, $y = n_y = m_y = 0$. And so the two matrices given in Eqs. (A1) and (A3) finally reduce to the following:

$$\left[\frac{\partial \nabla U}{\partial \mathbf{r}}\right]_{\mathbf{r}_0} = \begin{pmatrix} U_{xx} & 0 & U_{xz} \\ 0 & U_{yy} & 0 \\ U_{zx} & 0 & U_{zz} \end{pmatrix} \tag{A5}$$

and

$$\left[\frac{\partial \mathbf{a}_S}{\partial \mathbf{r}}\right]_{(\mathbf{r}_0, \mathbf{n}^a)} = -2\beta_0 \frac{m_0}{m} \frac{(1-\mu)}{r_1^5} \psi \begin{pmatrix} \frac{(x+\mu)}{r_1} m_x & 0 & \frac{z}{r_1} m_x \\ 0 & 0 & 0 \\ \frac{(x+\mu)}{r_1} m_z & 0 & \frac{z}{r_1} m_z \end{pmatrix} + \frac{1}{2}\beta_0 \frac{m_0}{m} \frac{(1-\mu)}{r_1^4} \begin{pmatrix} \frac{\partial \psi}{\partial x} m_x & 0 & \frac{\partial \psi}{\partial z} m_x \\ 0 & 0 & 0 \\ \frac{\partial \psi}{\partial z} m_z & 0 & \frac{\partial \psi}{\partial z} m_z \end{pmatrix} \tag{A6}$$

so that K in Eq. (36) can be calculated using Eqs. (A5) and (A6).

Acknowledgments

This work was funded by the National Center for Physics, Quaid-i-Azam University, Islamabad, Pakistan. We would like to acknowledge useful discussions with Thomas J. Waters.

References

[1] McInnes, C., McDonald, A., Simmons, J., and McDonald, E., "Solar Sail Parking in Restricted Three-Body Systems," *Journal of Guidance, Control, and Dynamics*, Vol. 17, No. 2, 1994, pp. 399–406. doi:10.2514/3.21211

[2] McInnes, C. R., "Artificial Lagrange Points for a Non-Perfect Solar Sail," *Journal of Guidance, Control, and Dynamics*, Vol. 22, No. 1, 1999, pp. 185–187.

[3] Morrow, E., Scheeres, D., and Lubin, D., "Solar Sail Orbit Operations at Asteroids," *Journal of Spacecraft and Rockets*, Vol. 38, No. 2, 2001, pp. 279–286.

[4] Baoyin, H., and McInnes, C., "Solar Sail Equilibria in the Elliptical Restricted Three-Body Problem," *Journal of Guidance, Control, and Dynamics*, Vol. 29, No. 3, 2006, pp. 538–543. doi:10.2514/1.15596

[5] Baoyin, H., and McInnes, C., "Solar Sail Halo Orbits at the Sun-Earth Artificial L1 Point," *Celestial Mechanics and Dynamical Astronomy*, Vol. 94, No. 2, Feb. 2006, pp. 155–171. doi:10.1007/s10569-005-4626-3

[6] Waters, T., and McInnes, C., "Periodic Orbits Above the Ecliptic in the Solar Sail Restricted 3-Body Problem," *Journal of Guidance, Control, and Dynamics*, Vol. 30, No. 3, 2007, pp. 687–693. doi:10.2514/1.26232

[7] Wan, C., "Solar Sail Geostorm Warning Mission Design," AAS Paper 04-107, Feb. 2004.

[8] Crison, M., and Dittberner, G., "Advanced Technologies for Future Environmental Satellite Systems," *13th Conference on Satellite Meteorology and Oceanography*, Paper 1.2, Norfolk, Virginia, 2004.

[9] McInnes, C. R., *Solar Sailing: Technology, Dynamics and Mission Applications*, Springer–Praxis Series in Space Science and Technology, Springer, London, 1999, pp. 250–256.

[10] Forward, R., "Statite: A Spacecraft That Does Not Orbit," *Journal of Spacecraft and Rockets*, Vol. 28, No. 5, 1991, pp. 606–611. doi:10.2514/3.26287

[11] Garbe, G., and Montgomery, E. E., "An Overview of NASA's Solar Sail Propulsion Project," AIAA Paper 2003-5274, July 2004.

[12] Morimoto, M., Yamakawa, H., and Uesugi, K., "Artificial Equilibrium Points in the Low-Thrust Restricted Three-Body Problem," *Journal of Guidance, Control, and Dynamics*, Vol. 30, No. 5, 2007, pp. 1563–1567. doi:10.2514/1.26771

[13] Morimoto, M., Yamakawa, H., and Uesugi, K., "Periodic Orbits with Low-Thrust Propulsion in the Restricted Three-Body Problem," *Journal of Guidance, Control, and Dynamics*, Vol. 29, No. 5, 2006, pp. 1131–1139. doi:10.2514/1.19079

[14] Leipold, M., and Götz, M., "Hybrid Photonic/Electric Propulsion," Kayser–Threde, GmBH Rept. SOL4-TR-KTH-001, Munich, Germany, Jan. 2002.

[15] Granata, J. E., Hausgen, P. E., Senft, D., Tlomak, P., and Merrill, J., "AFRL Thin Film Solar Cell Development and Upcoming Flight Experiments," *Proc. 2005 IEEE Aerospace Conference*, No. 1590, Big Sky, Montana, March 2005, pp. 1–6.

[16] Mengali, G., and Quarta, A., "Trajectory Design with Hybrid Low-Thrust Propulsion System," *Journal of Guidance, Control, and Dynamics*, Vol. 30, No. 2, March–April 2007, pp. 419–426. doi:10.2514/1.22433

[17] Wu, M., "On Stability of Linear Time-Varying Systems," *International Journal of Systems Science*, Vol. 15, No. 2, 1984, pp. 137–150.

[18] Skoog, R., and Lau, C., "Instability of Slowly Varying Systems," *IEEE Transactions on Automatic Control*, Vol. 17, No. 1, 1972, pp. 86–92. doi:10.1109/TAC.1972.1099866

[19] Råde, L., and Westergren, B., *Mathematics Handbook for Science and Engineering*, 3rd ed., Studentlitteratur, Sweden, 1995, pp. 64–65.

[20] McInnes, C., Eiden, M., Groepper, P., and Peacock, T., "Solar Sailing-Mission Opportunities and Innovative Technology Demonstration," ESA Bulletin 108, 2001, pp. 58–65.

[21] Wie, B., Murphy, D., Paluszek, M., and Thomas, S., "Robust Attitude Control Systems Design for Solar Sails, Part 1: Propellantless Primary ACS," AIAA 2004-5010, Aug. 2004.

[22] Gurfil, P., *Modern Astrodynamics*, 1st ed., Elsevier, London, 2006, pp. 189–207.

[23] Frisbee, R., "Advanced Space Propulsion for the 21st Century," *Journal of Propulsion and Power*, Vol. 19, No. 6, 2003, pp. 1129–1154.

[24] Gershman, R., and Seybold, C., "Propulsion Trades for Space Science Missions," *Acta Astronautica*, Vol. 45, Nos. 4–9, 1999, pp. 541–548. doi:10.1016/S0094-5765(99)00174-5

[25] Brophy, J., "Advanced Ion Propulsion Systems for Affordable Deep-Space Mission," *Acta Astronautica*, Vol. 52, Nos. 2–6, March 2003, pp. 309–316. doi:10.1016/S0094-5765(02)00170-4

[26] Kitamura, S., Ohkawa, Y., Hayakawa, Y., Yoshida, H., and Miyazaki, K., "Overview and Research Status of the JAXA 150-mN Ion Engine," *Acta Astronautica*, Vol. 61, 2007, pp. 360–366. doi:10.1016/j.actaastro.2007.01.010